Temperature Dependence of Current Density in Solid Oxide Fuel Cells

Rachel Thomas

Introduction & Motivation

This analysis explores the performance of a solid oxide fuel cell (SOFC) with increasing operating temperature from 800 to 1000ºC. SOFCs are an increasingly appealing option for utility scale integration of electrical grid supply. Given their characteristically high operating efficiency and fuel flexibility, SOFC's are uniquely suited to reduce greenhouse gas emissions relative to traditional coal generation plants. Additionally, there may be significant reductions relative to natural gas turbine generators due to methane leak during combustion and upstream leak during fracking and refinement. Moreover, the high operating temperature allows for waste heat to be recuperated in a bottoming cycle, or used directly as a bi-product in a combined power and heat generation plant. Ideally, a comprehensive SOFC analysis would compare the total electrical generation efficiency, to include the balance of plant and waste heat recovery, as a function of SOFC operating temperature. This model will provide a foundation for such future work, but will only explore immediate SOFC impacts. It has been shown that a higher operating temperature will increase the Gibbs free energy, but decrease overall electric potential. Of note, higher operating temperature would simultaneously decrease the SOFC lifespan due to accelerated material degradation; such collateral damage is acknowledged but will not be within the scope of this project.

Model formulation

A typical SOFC is modeled, consisting of a cement nickel dopped yttria-stabilized zirconia (YSZ) anode, lanthanum strontium manganite (LSM) cathode, and a YSZ electrolyte [1]. The fuel is assumed to be pure hydrogen, which is supplied to the anode; air is supplied to the cathode. The half-cell reactions, including surface vacancies, are as follows [2]:

Anode:

$$O^{2-}_{YSZ} + H_{Ni} \leftrightarrow [\ ]_{Ni} + OH^{-}_{YSZ} + e^{-}_{Ni} \quad (1)$$

$$OH^{-}_{YSZ} + H^{+}_{Ni} \leftrightarrow H_2O_{YSZ} + e^{-} \quad (2)$$

Cathode:

$$O_2 + 4e^{-} \leftrightarrow 2O^{2-} \quad (3)$$

Full Cell:

$$2H_2 + O_2 \leftrightarrow 2H_2O + 4e^{-} \quad (4)$$

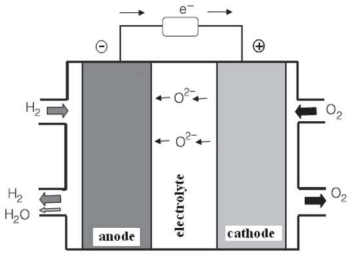

The impact of temperature variation is explored through a single particle model, with the anode and electrolyte each represented by one uniform volume. Positive sign convention is defined as positive charge moving to the positive electrode. This model defines only the anode and electrolyte, although similar trends will exist on the cathode side of the cell. The kinetics of the anode reactions, eq (1) and eq (2), are modeled independently to determine the total anode faradic current; this is best accomplished through the mass action kinetics form:

$$i_{\mathrm{Far}} = n_{\mathrm{elec}} F\left(q_{\mathrm{rop},1} + q_{\mathrm{rop},2}\right) \quad (5)$$

$$q_{\mathrm{rop}} = k_{\mathrm{fwd}} \prod_k C_{\mathrm{ac,k}}^{v'} - k_{\mathrm{rev}} \prod_k C_{\mathrm{ac,k}}^{v''} \quad (6)$$

$$k_{\mathrm{fwd}} = k^*_{\mathrm{fwd}} \exp\left(-\frac{\beta n_{\mathrm{elec}} \mathrm{F} \Delta\phi_{an}}{\mathrm{RT}}\right) \quad (7)$$

$$k^*_{\mathrm{fwd}} = A_{\mathrm{fwd}} \exp\left(-\frac{E_{act}}{RT}\right) \quad (8)$$

$$k_{\mathrm{rev}} = k_{\mathrm{fwd}} \exp\left(\frac{\Delta G_{\mathrm{an}}}{\mathrm{RT}} + \frac{n_{\mathrm{elec}} \mathrm{F} \Delta\phi_{an}}{\mathrm{RT}}\right) \quad (9)$$

i_{Far} is the faradic current generated by reactions at an electrode [A], F is faraday's constant [C/kmol], q_{rop} is the reaction's rate or progress [kmol/m-s], $C_{\mathrm{ac,k}}^{v'}$ is the activity concentration of the reactants while $C_{\mathrm{ac,k}}^{v''}$ is the activity concentration of the products, β is the unitless forward charge-transfer reaction rate, n_{elec} is the electrons transferred per reactant, $\Delta\phi_{an}$ is the electric potential difference between the anode and the cathode [V], R is the universal gas constant, and T is the temperature [K].

ΔG_{an} is the Gibbs free energy of the reaction [J/kmol], which is a function of the molecular thermodynamics as follows:

$$\Delta G_{\mathrm{an}} = \Delta G^{\mathrm{o}}_{\mathrm{an}} - \mathrm{R}T \prod_k C_{\mathrm{ac,k}}^{v''-v'} \quad (10)$$

$$\Delta G^{o}_{\mathrm{an}} = \sum_{\mathrm{k}} g^{o}_{prod} - \sum_{\mathrm{k}} g^{o}_{react} \quad (11)$$

$$g^{o}_{k} = h_{\mathrm{k}} - T s_{\mathrm{k}} \quad (12)$$

g^{o}_{k} is calculated using the enthalpy (h [J/kmol]) and entropy (s [J/kmol-K]) values shown in Table I below, at atmospheric pressure and 800ºC. While the species enthalpy and entropy will change slightly with increased temperature, it's effect over the studied range of 800ºC to 1000ºC is assumed to be negligible. The increased temperature will be accounted for through the Gibbs free energy, eq (12).

Table I: Species Thermodynamic Properties

Species	Enthalpy [kJ/mol]	Entropy [J/mol-K]
H on Ni surface	-9.1	80.2
Vacancy on Ni surface	20.0	33.1
O^{2-} ion on YSZ surface	-122.3	128.9
OH^{-} ion on YSZ surface	47.8	165.9
H_2O on YSZ surface	-293.4	177.0

Table 2 includes all other constants used in the model; experimentally derived parameters are derivative of those used in [3]. The molar fractions of each species, X, are assumed variables. Those impact of varied molar fractions are being studied in a parallel model by Lydia Meyer.

Table II: Physical and Electrochemical Properties

Property	Variable	Value
Molar fraction of H on Ni surface	$X_{H,Ni}$	0.9
Molar fraction of vacancy on Ni surface	$X_{Vac,Ni}$	0.1
Molar fraction of hydroxyl ion on YSZ surface	$X_{OH,YSZ}$	0.4
Molar fraction of O^{2-} ion on YSZ surface	$X_{O2-,YSZ}$	0.4
Molar fraction of vacancies on YSZ surface	$X_{Vac,YSZ}$	0.1
Molar fraction of H_2O on YSZ surface	$X_{H2O,YSZ}$	0.1
Activation energy, eq (1)	$E_{act,1}$	90.0 [kJ/mol]
Activation energy, eq (2)	$E_{act,2}$	90.0 [kJ/mol]
Arrhenius rate coeff, eq (1)	$A_{fwd,1}$	$1•10^{11}$ [m^3/kmol-s]
Arrhenius rate coeff, eq (2)	$A_{fwd,2}$	$1•10^{10}$ [m^3/kmol-s]
Double layer capacitance	$C_{dl,an}$	0.003 [F/m^3]
Transfer coefficient	$\alpha_{fwd,1}$	0.5
Transfer coefficient	$\alpha_{fwd,2}$	0.5
Surface concentration	γ_{sur}	1•10-9 [kmol/m^2]
External current	i_{ext}	1000 [A/m^2]

There is one major deviation from the published values which estimates the surface concentration to be $1•10^9$ [mol/cm^2] or 10 [kmol/m^2] [3]. The plots shown within will should follow the same general trends despite the disparity in surface concentration, although the values would differ significantly. The impacts of this change (and difficulties associated with programming the published value) are analyzed in the 'Results and Discussion' section.

The cell is assumed to have a fixed gas phase composition and zero transport limitations, as would be expected in a flooded cell, the state variable consists only of the anode electric potential double layer, $\Delta\phi_{\mathrm{dl,an}}$, as calculated in eq (12). Modeling the double layer as a capacitor yields the time differential, eq (14), which is solved for $i_{\mathrm{dl,an}}$.

$$\Delta\phi_{\mathrm{dl,an}} = \phi_{\mathrm{elyte}} - \phi_{\mathrm{an}} \quad (13)$$

$$C_{\mathrm{dl,an}} = \frac{Q_{dl,an}}{\Delta\phi_{\mathrm{dl,an}}} \quad (14)$$

$$\frac{\partial\Delta\phi_{\mathrm{dl,an}}}{\partial t} = \frac{\partial \mathrm{Q}_{\mathrm{dl,an}}}{\partial t}\frac{1}{C_{\mathrm{dl,an}}} \quad (15)$$

$$\frac{\partial\Delta\phi_{\mathrm{dl,an}}}{\partial t} = \frac{i_{\mathrm{dl,an}}}{C_{\mathrm{dl,an}}} \quad (16)$$

$$i_{\mathrm{dl,an}} = i_{\mathrm{ext}} - i_{\mathrm{Far,an}} \quad (17)$$

An external current of 1,000 [A/m^2] is a defined constant while analyzing the impact of temperature on the current density. In the subsequent section, the SOFC's polarization curve is extrapolated by varying the current density from 0 to 3,000 [A/m^2].

Results & Discussion

The Gibbs free energy for each anodic equation is plotted in Figure 1. Interestingly, eq (1) yields a positive Gibbs free energy while eq (2) yields a negative Gibbs free energy. This means that the second reaction will occur spontaneously but the first one would not. This is not possible as each reaction need to occur at a similar rate to avoid species build up. As can be seen by the summation line in the plot, the total reaction rate is negative, which is expected for an energy producing cell. The temperature variation has minimal impact on the Gibbs free energy, as can be seen by the nearly flat slopes of each line. When looking at the total anodic Gibbs free energy (the summation line) it decreases from -115.0 to -115.4 kJ/mol, meaning the reaction becomes more favorable with increased temperature. This is a relatively small change,

accounting for a 0.35% increase in energy per mole of reactant.

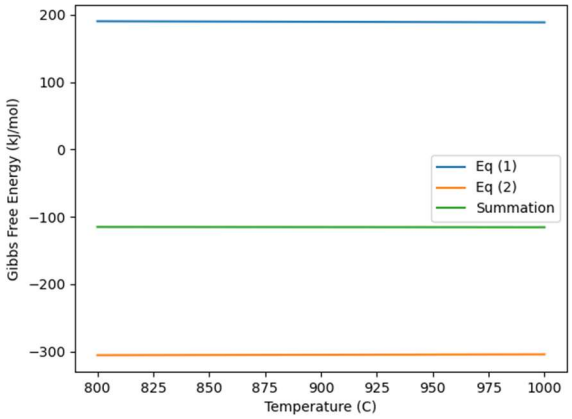

Figure 1: Temperature Dependence of Gibbs Free Energy

The major advantage of using the mass action kinetics over the Butler-Volmer form for calculating current density is the ability to account for the multistep reactions occurring on the triple phase boundary of the anode. If this were instead modeled using a global reaction, the cell's potential and current density would be overestimated, because energy lost in the intermediate reactions is not accounted for. Further complexities beyond the scope of this model may yield additional limiting factors, such as the rate of gas diffusion to the reaction site.

However, modeling the anodic reactions independently becomes difficult when the sign of the Gibbs free energy for each reaction is different. In particular, the Gibbs free energy feeds into the reverse reaction rate as calculated in eq (9). Because the Gibbs free energy is inside an exponential function, eq(1) yields a positive term for $\frac{\Delta G_{\mathrm{an}}}{\mathrm{RT}}$ while $\frac{n_{\mathrm{elec}}\mathrm{F}\Delta\phi_{an}}{\mathrm{RT}}$ is negative. If the sum of those terms is negative, the exponential will decrease, but if the sum is positive, the exponential will yield an overflow error. Conversely, for eq (2), both terms are negative. This leads to significant stability issues in the model, and is the primary reason the value of gamma could not be readily adjusted to match the literature values.

As can be seen through the curves in Figure 2, each temperature will reach a steady state electric potential within a millisecond. The rate at which the double layer potential reaches its equilibrium voltage is a directly correlated to the capacitance of the material. When a material has a larger capacitance, a larger double layer current can develop and more charge can be stored before a steady state is obtained.

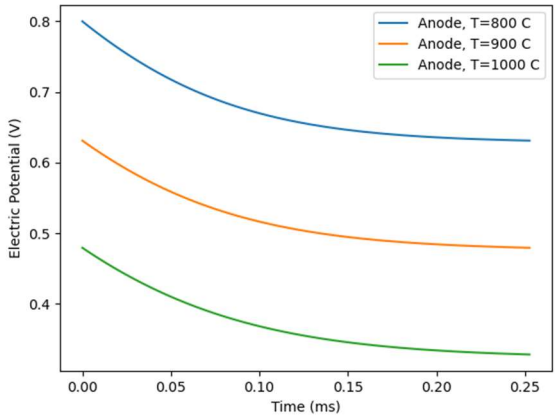

Figure 2: SOFC Electric Potential

The results of the model yield decreasing cell potential at increased temperatures. This result is surprising (aka probably wrong…?) as increased temperature generally yields faster kinetics and increased cell potential. As calculated in this model, k^{*}_{fwd} decreases with increased temperature, as the negative number in the exponent in eq (8) becomes smaller. k_{fwd} decreases at a faster rate due to a direct relationship with k^{*}_{fwd} and due to a decreasing, positive number in the exponential of eq (7). Following the same logic, k_{rev} will decrease, but at a slower rate than k_{fwd}. The cumulative result is an increase in the reaction rate of progress, q_{rop} as calculated in eq (6), and subsequently an increase in the faradic current. Because the external current is constant, an increase in the faradic current correlates to a decrease in the double layer current density as calculated in eq (17).

Finally, the model was run at varied external current densities from 0 to 3000A/m^2, for a defined cell temperature of 800ºC; results are shown below in Figure 3. At low external current densities, the anodic double layer current is driven by the faradic current. For example, at an external current, eq (16) and eq (17) simplify as follows:

$$\frac{\partial\Delta\phi_{\mathrm{dl,an}}}{\partial t} = \frac{i_{\mathrm{Far,an}}}{C_{\mathrm{dl,an}}} \tag{18}$$

The anode faradic current density is independent of the external current. Therefore, the cell's potential is maximized when the external current is 0 A/m2. As the external current is increased, and the constant faradic current is subtracted, the double layer current decays. At increased external voltages, it would be expected that i_{ext} would exceed $i_{\mathrm{Far,an}}$, thus leading to a positive value for the double layer current and an inflection in the polarization curve whereby further increases in i_{ext} would result in rapid decrease of electric potential and cell performance.

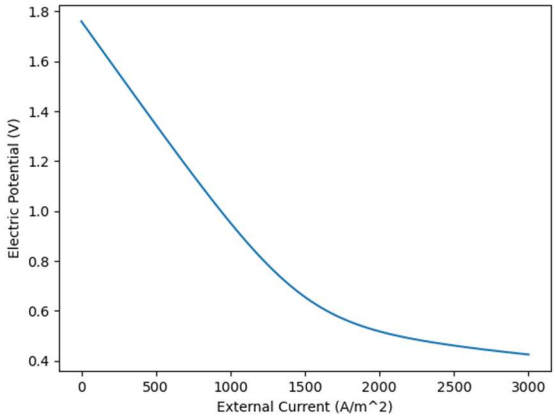

Figure 3: Polarization Curve

Conclusion

These results show that an increase in cell operating temperature yields significant reductions in the cell potential. Operating at 1000ºC, a 20% increase over the base scenario of 800ºC, results in a 46% decrease in electrical potential, from 0.632V to 0.303V. This does not agree with the conventional wisdom that cell potential increases with temperature. The polarization curve reflected decreasing cell potential with increased external current density, decaying to a value of approximately 0.4V.

The scope of this analysis admittedly quite narrow, most notably by not accounting for the cathode. It is possible that with the integration of specific cell geometry and an accurate gamma value (and commanding wizardry of python, to which the author is severely deficient), that the result would better align with other published findings. As scientists and engineers continue to increase SOFC operating temperature as new materials allow, it is essential to model the holistic system impacts. The trade off in performance must be balanced with the increased load demand for the balance of the plant.

References

[1] T. F. Fuller and J. N. Harb, "Fuel-Cell Fundamentals," in *Electrochemical Engineering*, Hoboken, NJ, John Wiley & Sons, 2018, pp. 195-222.

[2] J. Santos and T. Matencio, "Ceramic Materials for Solid Oxide Fuel Cells," Universidade Federal de Minas Gerais, Brazil, 2018.

[3] S. C. DeCaluwe, H. Zhu, R. J. Kee and G. S. Jackson, "Importance of Anode Microstructure in Modeling Solid Oxide Fuel Cells," *Journal of the Electrochemical Society,* vol. 155, pp. B538-B546, 2008.

[4] E. Weidner, R. Ortiz Cebolla and J. Davies, "Global deployment of large capacity station fuel cells - Driver of, and barriers to, stationary fuel cell deployment, EUR 29693 EN," Publication Office of the European Union, Luxembourg, 2019.

[5] U.S. Department of Energy, "Report on the Status of the Solid Oxide Fuel Cell Program," Washington, DC 20585, 2019.

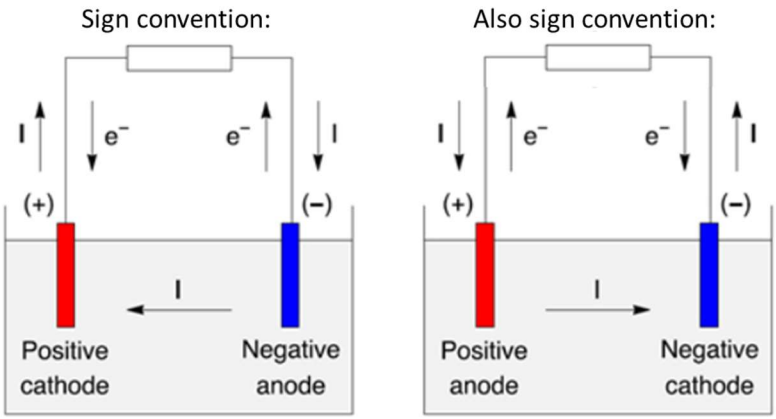

Because SCIENCE! (...is moody)

Eh, it's 2020... you do you...